Recent Highlights from BRAHMS

I.G. Bearden,
Niels Bohr Institute
for the BRAHMS Collaboration‡

In order to fully understand the physics involved in ultrarelativistic collisions it is necessary to explore as much of the phase space as possible. Doing so provides both an experimental and theoretical challenge as one moves to larger rapidities. Experimentally, because, for example, beam related backgrounds become more severe and mean particle momenta increase rapidly for a given transverse momentum. Theoretically, since as one moves away from midrapidity one can no longer rely on the assumption of Bjorken invariance and one must begin to work in three spatial dimensions rather than two. Additionally, different effects must play as one moves from the relatively net–baryon poor region around mid–rapidity toward forward rapidity where there is substantial baryon number. This proceeding will concentrate on the experimental work done by the BRAHMS collaboration in trying to characterize particle production over the rapidity range from y=0 to y=3.5. We present results [1] on charged hadrons as well as identified particles ($\pi^{\pm}$, $K^{\pm}$, $p^{\pm}$) for both low p_T (< 1.5GeV/c) and high p_T (> 2GeV/c).

The high p_T results allow us to characterize the so-called high p_T suppression from midrapidity to $y_\pi = 3.5$ for Au+Au and Cu+Cu at both $\sqrt{s_{NN}} = 200$ GeV and $\sqrt{s_{NN}} = 62.4$ GeV. This is done by comparing spectra for the nucleus-nucleus collisions to those from proton-proton collisions; thus, we have collected data from p+p at both $\sqrt{s_{NN}} = 200$ GeV and $\sqrt{s_{NN}} = 62.4$ GeV. In addition, the p+p results allow for comparisons with perturbative QCD calculations, a subject not covered in the present work but which is discussed elsewhere[3]. Measurements at low p_T allow us to measure the yields of $\pi^{\pm}$, $K^{\pm}$, $p^{\pm}$, and thus the "chemistry" of the produced matter as a function of rapidity.

The BRAHMS experiment consists of two movable magnetic spectrometers, covering -0.1$< \eta <$3.9, and a set of detectors to determine the multiplicity of charged particles and the interaction point [4]. For the p+p collisions additional Čherenkov radiators, positioned around the beam pipe at $\pm$1.9 m and $\pm$6.4 m from the nominal interaction point, were used to determine the interaction vertex to a resolution of ~ 2 cm. These detectors cover approximately 12 mb (for p+p at $\sqrt{s_{NN}} = 62.4$ GeV out of the total 36 mb cross section.

Jet quenching in heavy ion collisions at the RHIC top energy is generally considered a prime indicator of the creation of strongly interacting quark gluon matter[2]. In heavy ion collisions at $\sqrt{s_{NN}} = 200$ GeV, strong suppression of high p_T hadrons has been

‡ For the full author list and acknowledgements see the appendix of this volume.

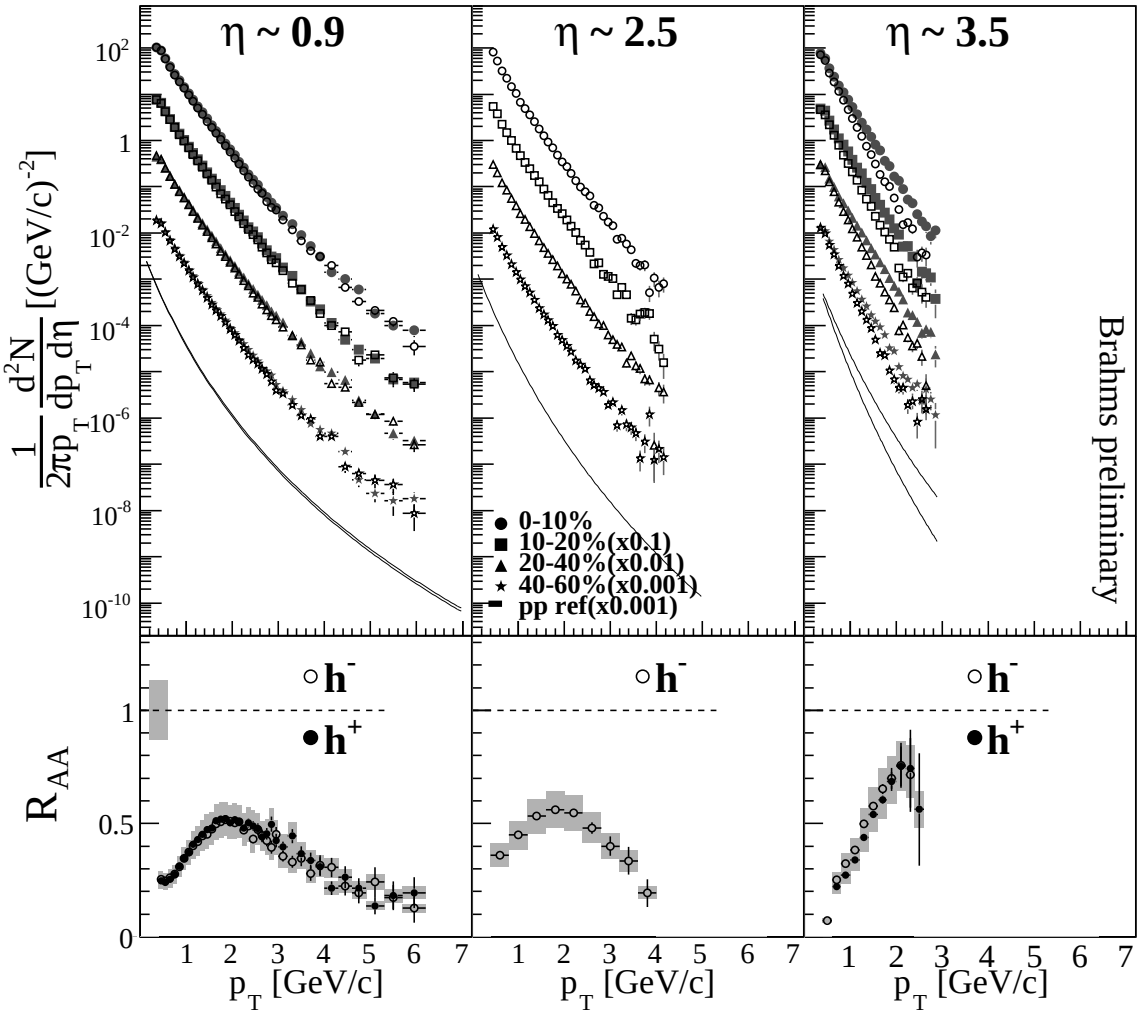

Figure 1. The middle panels show charged hadron spectra for several centralities from $\sqrt{s_{NN}}$ = 200 GeV Au+Au collisions at eta=0.9,2.5, and 3.5 from left to right. Filled and open symbols are for positive and negative hadrons, respectively. The full drawn lines are fits to the measured p+p spectra, and tin the rightmost panel, the upper line is the spectrum of positive hadrons. The bottom panels show R_{AA} for the most central data. The shaded bar at 1 show the error on the scale.

observed, saturating from $p_{\rm T} \simeq 4$ to ~ 20 GeV/c. The results of experiments using $d-Au$ collisions at this energy, and which show no suppression at midrapidity, indicate that the suppression is a final state effect, thought to be due to energy loss in a produced medium characterized by a high density of colour charges. The partons lose energy through gluon emission leading to a depletion of high $p_{\rm T}$ hadrons. In order to better understand these mechanisms measurements have been done at both $\sqrt{s_{NN}} = 200$ GeV and $\sqrt{s_{NN}} = 62.4$ GeV, with a variety of collision systems. Measuring the nuclear modification factor as a function (pseudo)rapidity should give a more clear picture of the extent of the high–density medium produced.

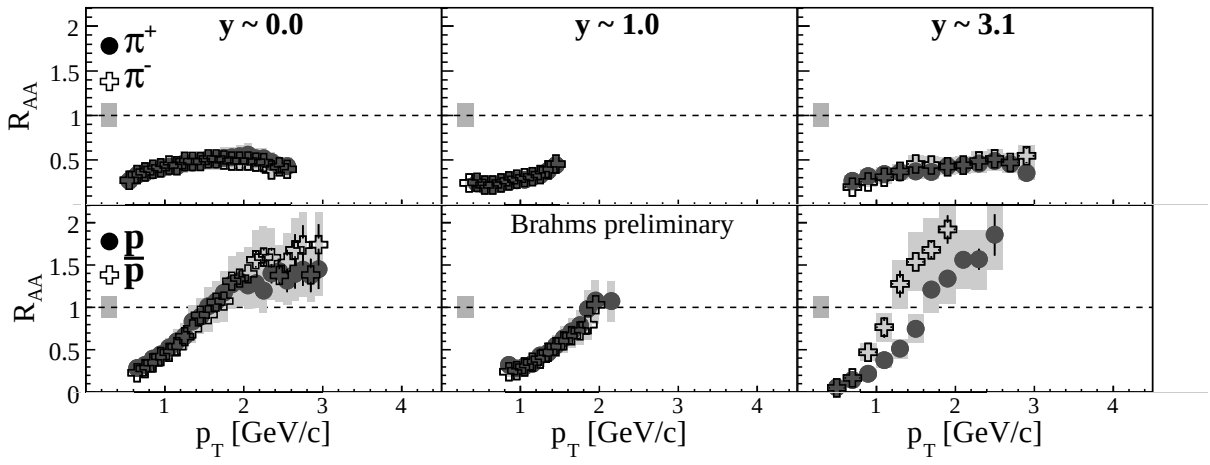

Figure 2. R in $\sqrt{s_{NN}}$ = 200 GeV Au+Au for identified pions and protons. The shaded bar at 1 show the error on the scale.

In figure 1, we present spectra obtained using the BRAHMS spectrometers for several centralities (as noted in the figure) at pseudorapidities 1,2.5, and 3.5. We also have results at 0 and 3, but these are not included in the figure. The spectra shown as full drawn lines are from p+p collisions. The lower panel shows the nuclear modification factor for the 10% most central data. The nuclear modification factor is defined to be:

$$R_{AA}(\eta, p_{\mathrm{T}}) = \left(\frac{d^2N^{AA}}{\langle N_{bin}^{AA}\rangle\, dp_T d\eta}\right) \cdot \left(\frac{d^2N^{pp}}{dp_T d\eta}\right)^{-1} \tag{1}$$

where $\langle N_{bin}^{AA}\rangle$ is the number of binary collisions in an A-A collision given by a Glauber model calculation. For all rapidities, the R_{AA} reaches a maximum value at $p_{\mathrm{T}} \approx 2GeV/c$, and then decreases. The results are consistent within our uncertainties for all pseudorapidities measured. One notes that the underlying spectra themselves change with pseudorapidity, and that as one moves forward the positive and negative particles are no longer equivalent. There are more positives at forward rapidity, due to the the presence of a larger number of protons in both p+p collisions and Au+Au collisions.

Figure 2 shows that both positive and negative pions exhibit the suppression at all measured rapidities, while the protons and antiprotons show an enhancement compared to binary scaling above $p_{\mathrm{T}} \approx 1.8GeV/c$. Again, we see no significant change between the mid and forward rapidities.

A similar analysis has been performed on data at $\sqrt{s_{NN}}$ = 62.4 GeV for both Au+Au and Cu+Cu collisions. Here also, the results do not change as one moves forward in rapidity, as can be seen in figure 3, which shows BRAHMS results from Au+Au for $\eta = 0, 0.9, 3.1$. One notes that at this energy the large suppression seen for top energy Au–Au collisions is not present in these data. This is discussed in greater detail in [5].

A possible explanation of this constant behaviour with respect to rapidity has

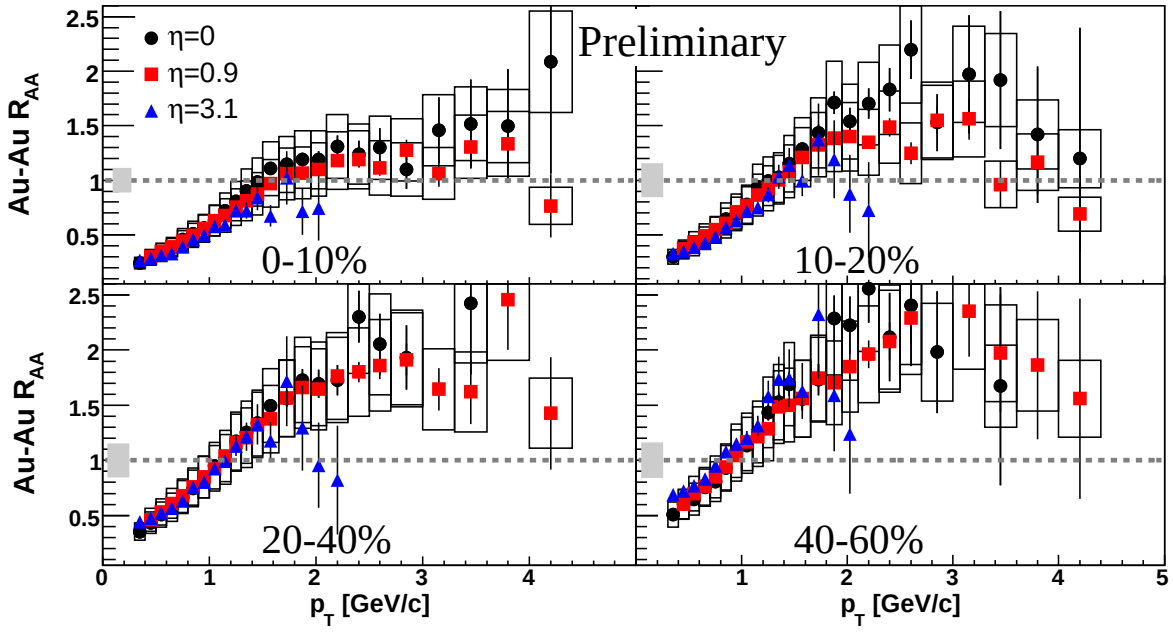

Figure 3. R_{AA} for Au-Auu collisions at $\sqrt{s_{NN}} = 62.4$ GeV for charged hadrons. The shaded bar at 1 show the error on the scale. Circles are data at midrapidity, squares at $\eta = 0.9$, and triangles at $\eta = 3.1$. The centrality classes are given in the figure.

been published recently[6]. Here, the authors include nuclear effects such as shadowing and multiple scattering in perturbative QCD calculations (which are shown to agree with the BRAHMS d+Au results discussed below, and a reasonable initial geometry of homogeneous deconfined (i.e. 'colored') matter which is initially very thin in the longitudinal direction. Jets emitted transversely, then, will see more deconfined matter than those emitted longitudinally since the longitudinally emitted particles see only a thin slice of this matter before reaching the surface, with which the jet will co-move. Thus, the forward suppression is explained as a conspiracy of initial state (e.g. shadowing) and final state (suppression in the thin slice of deconfined matter) effects.

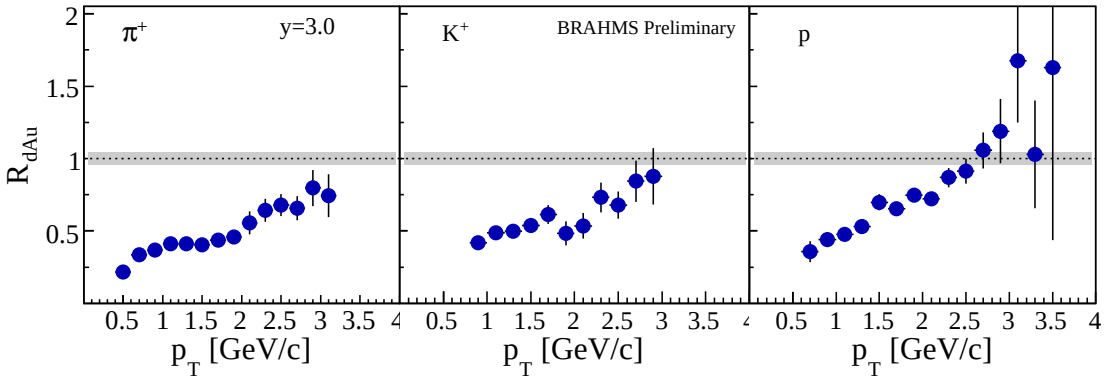

Figure 4. Nuclear modification factors, R_{dAu}, for (from left) pions, kaons, and protons for d+Au at $y = 3$ at $\sqrt{s_{NN}} = 200$ GeV. The shaded bar at 1 indicates the error on the scale.

For symmetric heavy–ion collisions, we see no significant changes from midrapidity to the most forward rapidities we measure. For d+Au collisions, however, there is a change over this rapidity range as reported by BRAHMS in [6]. The transition from an enhancement at midrapidity to a clear suppression with increasing rapidity in $d + Au$ collisions indicates another mechanism, related to the nuclear initial state. Theoretical work has predicted an effect similar to this on the basis of gluon–saturation phenomena, a scenario known as the Color Glass Condensate [7]. In fact, more recent calculations[8] using this framework are able to reproduce the BRAHMS data reasonably well. In figure 4 we present recent results on identified particles at the highest rapidity measured, 3, which show a similar pattern as for mid–rapidity Au+Au collisions, namely, the mesons exhibit a suppression. Here, though, one notes that protons are, for a given transverse momentum, at roughly the same level as mesons.

BRAHMS has collected very large data sets at low transverse momentum also, allowing for a detailed study of the bulk properties of the produced matter as a function of rapidity. One notes that in the rapidity range covered by BRAHMS, the charged particle density decreases by roughly 30%, and the net–proton density increase by a factor of two. Given this, one might expect other variables to change as well; however, as we have already seen in the case of high– p_{T} suppression, this is not necessarily the case.

In figure 5, we show the elliptic flow v_2 as a function of p_{T} . One notes no significant change over 3 units of rapidity for either pions or protons, and this despite the observed difference of about 35% in this range for the integral v_2. This indicates that the eccentricity and resulting pressure gradients remain rather constant over this broad rapidity range. This implies, then, that the decrease in the integral v_2 is due to the softening of the spectra at forward rapidities.

At a much later stage of the collision, protons and neutrons may coalesce to form deuterons. Since deuterons are only very weakly bound, those surviving to our detectors must have been formed in the very late stages of the collision. The ratio of the invariant cross section of deuterons to the square of the invariant cross section of protons defines the coalescence parameter, B_2, which can be related to the volume of homogeneity of the emitting source. Thus, by measuring this experimental parameter as a function of rapidity, we obtain information on how the volume changes. We present, in figure 6, the results from $\sqrt{s_{NN}} = 200$ GeV Au+Au collisions. Here again, one notes that there is no significant change from y=0 to y=3. One notes also that these results are very similar to those from $\sqrt{s_{NN}} = 17$ GeV[9]. The volume of homogeneity seems to be remarkably independent of both energy and rapidity.

Figure 7 shows the net–proton density $dN/dy(p) - dN/dy(\bar{p})$ as a function of rapidity for $\sqrt{s_{NN}} = 62.4$ GeV Au+Au collisions. This distribution changes dramatically as $\sqrt{s_{NN}} =$ GeV increases. At RHIC, the net–proton density is $6.4 \pm 0.4 \pm 1.0$ near mid–rapidity ($y < 1$) and increases to $12.4 \pm 0.3 \pm 3.2$ at $y \sim 3$ for the top energy, indicating a higher degree of transparency than at AGS and SPS. The more recent data from $\sqrt{s_{NN}} = 62.4$ GeV Au+Au collisions confirms this picture as well as the extrapolation

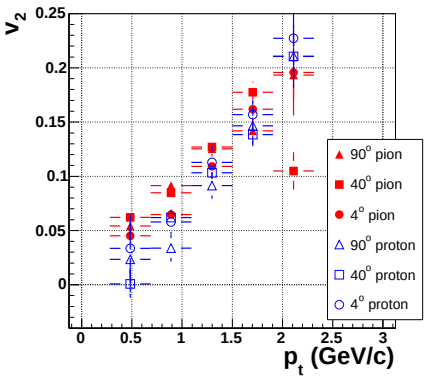

Figure 5. $v_2(p_T)$ vs p_t for pions and protons at $\eta = 0, 1$, and 3 (labelled 90, 40 and 4 degrees in the figure).

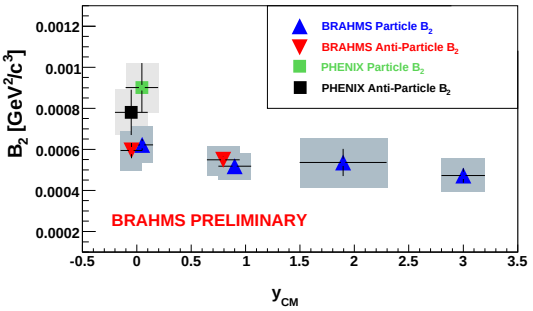

Figure 6. Experimental B_2 vs.rapidity for both particles and anti–particles. Neither shows a change with rapidity, indicating that the transverse size of the emitting source is constant.

from the highest measured rapidity to beam rapidity used in the higher energy data. At this lower energy, BRAHMS covers a larger fraction of the total rapidity range; in fact, we are able to measure data in the so-called fragmentation region where the 'primordial' baryon number density is highest, as can be seen in the figure. We observe that the net proton density rises from 12 at midrapidity to 30 at $y = 2.3$. The nuclear stopping is quantified by the rapidity loss $\langle \delta y \rangle$, which, for mass symmetric collisions, is defined by $\langle \delta y \rangle = y_b - \langle y \rangle$, where $\langle y \rangle$ is the mean net–baryon rapidity after the collision:

$$\langle y \rangle = (\frac{dN}{dy})^{-1} \int_0^{y_b} y \frac{dN_{(B-\bar{B})}(y)}{dy} dy \qquad (2)$$

requiring the entire net–baryon distribution. Corrections for neutrons as well as strange baryons such as Λ's and Σ's are obtained via MC. Details can be found in [10, 11]. Since the data do not cover the entire rapidity range, we extrapolate by fitting with a continuous function with area equal to the number of participants (357 ± 9 for the 5% most central). Doing this, we find $\langle \delta y \rangle = 2.16 \pm 0.05$ for $\sqrt{s_{NN}} = 62.4$ GeV and $\langle \delta y \rangle = 2.0 \pm 0.2$ for $\sqrt{s_{NN}} = 200$ GeV. These BRAHMS results, together with results from earlier experiments at the AGS and SPS are shown in figure 8. Using these data, one can extrapolate to LHC energy. We have done this by fitting the rapidity loss as a function beam rapidity assuming a simple continuous function ($\langle \delta y \rangle = A + B(1 - \exp y_{beam}$), which gives a lower limit in rapidity loss of $\langle \delta y \rangle \approx 2.1$. For comparison, we show a linear extrapolation from AGS and SPS (dotted line) and from SPS and low energy RHIC. Presumably, the latter linear extrapolation gives an upper limit on the rapidity loss to be expected at LHC, which then must lie between 2 and 3 units of rapidity.

In addition to data for protons and antiprotons, we have data for light mesons as well. Using the yields of these together with the protons, we can—with the help of statistical model calculations—explore the variation of chemical potential and chemical

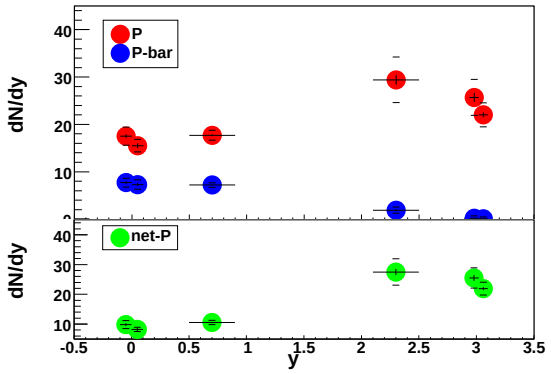

Figure 7. The upper panel contains the proton (open) and anti–proton(filled) rapidity densities from $\sqrt{s_{NN}}$ = 62.4 GeV Au+Au collisions. The net–proton rapidity density is plotted in the lower panel.

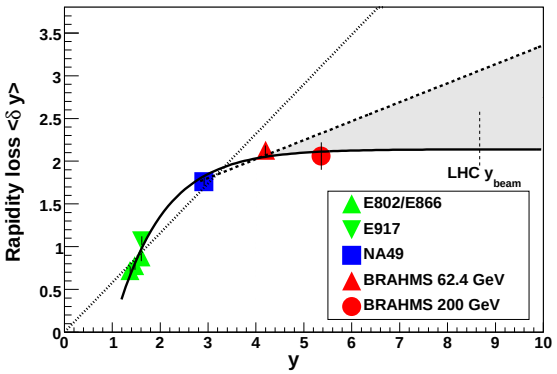

Figure 8. Rapidity loss as a function of beam rapidity relative to the colliding system's center of mass. The curves are a linear fit to 'low energy' AGS and SPS results (dotted), a linear fit to SPS and RHIC results (dashed), and an exponential function (full drawn line) described in the text.

freeze–out temperature as a function of rapidity. Calculations indicate that the chemical freeze–out temperature is essentially constant ($T \approx 170 MeV$ from SPS energy up to top RHIC energy and constant over the measured rapidity range at RHIC. The baryon chemical potential, however, changes from above 250MeV at SPS to roughly 20MeV for midrapidity at the top RHIC energy.

Rather than rely explicitly on such calculations, one can use the antiproton to proton ratio as the independent variable rather than a calculated quantity such as temperature or chemical potential. So doing, one finds that all available data for $\frac{K^-}{K^+}$ vs $\frac{p-}{p}$ fall along a universal curve [12]. One finds also that at the most forward rapidities for RHIC data at $\sqrt{s_{NN}}$ = 62.4 GeV the ratio $\frac{\bar{p}}{p}$ is similar to that at SPS energies. Thus, it is possible to compare results from SPS to RHIC as a function of $\frac{\bar{p}}{p}$. In figure 10, we plot the kaon to pion ratio as a function of $\frac{\bar{p}}{p}$. One sees that for both the positive and negative mesons, the BRAHMS data from $\sqrt{s_{NN}}$ = 62.4 GeV are consistent with data from SPS at the same value of $\frac{\bar{p}}{p}$. The same holds true for the inverse slope of an exponential fit to the kaon spectra, as seen in 9.

In conclusion, BRAHMS has measured charged hadron spectra from a variety of systems at both $\sqrt{s_{NN}}$ = 62.4 GeV and $\sqrt{s_{NN}}$ = 200 GeV, both as a function of pseudorapidity and centrality. Our measurements cover an extensive part of phase space, including the forward rapidity region. Through the nuclear modification factors R_{AuAu} and R_{dAu} we have found a suppression of high–p_T particle production in $d + Au$ collisions at forward rapidities, in contrast to the enhancement previously seen at midrapidity. R_{dAu} also contrasts to R_{AA} in that it changes with increasing rapidity, while R_{AA} shows very little variation with rapidity. We also find a suppression of R_{AuAu} at high–p_T in central collisions, extending at least 3.5 units of pseudorapidity away

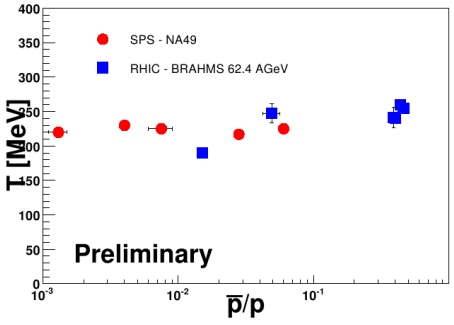

Figure 9. Inverse slope parameter from exponential fits to kaon spectra. Circles represent data from NA49, squares BRAHMS data.

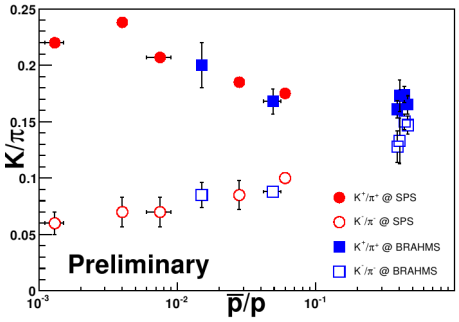

Figure 10. Ratio of kaons to pions versus antiprotons to protons. Circles are data from NA49, while squares are BRAHMS data. Filled symbols denote positive particles, open symbols negative particles. Note that the x-axis is logarithmic.

from $\eta = 0$. The situation for identified particles is the same, there is no significant difference from mid to forward rapidity. We have measured the net–proton rapidity density at both $\sqrt{s_{NN}} = 62.4$ GeV and $\sqrt{s_{NN}} = 200$ GeV, which can be related to the rapidity loss (or, equivalently, the energy loss) of the incident nucleons. For the lower energy data, we cover well into the fragmentation peak, so the uncertainties on the calculated rapidity loss are much smaller than for the top energy where we have a more uncertain extrapolation. The rapidity loss is constant within our uncertainties for these two energies. Our forward meson results for $\sqrt{s_{NN}} = 62.4$ GeV are remarkably similar to results from the SPS, which might lead one to infer that the baryon chemical potential is driving factor in the changes seen from mid to forward rapidity, or from RHIC top energy to SPS energies.

References

[1] See also other BRAHMS contributions contained in these proceedings.
[2] "First Three Years of Operation of RHIC", Nucl. Phys. **A757**, Issues 1-2 (2005).
[3] I.Arsene *et al* , hep-ex/0701041, submitted to Phys. Rev. Lett.
[4] M. Adamczyk *et al* , Nucl. Instr. Meth. **A499**, 437 (2003).
[5] T.M. Larsen, these proceedings.
[6] BRAHMS Collaboration, , I. Arsene *et al* , Phys. Rev. Lett. **93**, 242303 (2004).
[7] L. McLerran and R. Venugopalan, Phys. Rev. D **49**, 2233(1994), Phys. Rev. D **49**, 3352 (1994), Phys. Rev D **50**, 2225 (1994), Phys. Rev. D **59**, 094002 (1999); Y. V. Kovchegov, Phys. Rev. D **54**, 5463 (1996), Phys. Rev. D **55**, 5445 (1997).
[8] D. Kharzeev et al. Phys. Lett. **B599**, 23, (2004)
[9] I. G. Bearden *et al.*, Phys. Rev. Lett. **85** 2681 (2000),I. G. Bearden *et al.*, Eur.Phys.J. **C23** 237 (2002) .
[10] I. G. Bearden *et al.*, Phys. Rev. Lett. **93** 102301 (2004).
[11] P. H. L. Christiansen, Ph.D. thesis, University of Copenhagen, 2003.
[12] I. G. Bearden *et al.*, Phys. Rev. Lett. **90** 102301 (2003).